A TECHNIQUE FOR BLOOD DETECTION IN WIRELESS CAPSULE ENDOSCOPY IMAGES

Barbara Penna, Tammam Tillo†, Marco Grangetto‡, Enrico Magli*, Gabriella Olmo**

* Dip. di Elettronica
Politecnico di Torino,
C.so Duca degli Abruzzi, 24
10129 Torino, Italy
Ph.: +39-011-5644094
Fax: +39-011-5644149
name.surname@polito.it

‡Dip. di Informatica
Università degli Studi di Torino
C.so Svizzera, 185
10149 Torino, Italy
Ph.: +39-011-6706711
Fax: +39-011-751603
marco.grangetto@di.unito.it

†Dept. of Electrical and Electronic Eng.
Xi'an Jiaotong Liverpool University
111 Ren Ai Road
Suzhou, Jiangsu Province, China 215123
Ph.: +86 512 8816 1408
Fax: +86 512 8816 1999
tammam.tillo@xjtlu.edu.cn

ABSTRACT

Wireless capsule endoscopy is an innovative technology for visualizing anomalies in the gastrointestinal tract, useful to replace traditional endoscopic diagnosis. Its advantages are related to the capability to reach the duodenum and small intestine, while eliminating the discomfort of patients. The time spent by a physician analyzing the results of wireless capsule endoscopy video can vary between 45 and 180 minutes, limiting its widespread diffusion. Therefore, methods able to perform an automatic pre-screening of images of interest are necessary. This paper presents an innovative technique to detect bleeding regions in wireless capsule endoscopy video. Experimental results show that the proposed algorithm exhibits a low false alarm rate, and is effective at reducing the time needed to analyze video sequences.

1. INTRODUCTION

The Wireless Capsule Endoscopy (WCE) is a non-invasive technique that enables the visualization of the small bowel mucosa for diagnosing purposes. The WCE is swallowed by the patient and it is passively propelled by peristalsis. The most common indication for capsule endoscopy is for evaluation of obscure gastrointestinal bleeding. Early systematic studies suggest that it is a very effective diagnostic tool in patients with Crohn's disease; moreover, it is expected that WCE would offer a clinical benefit in terms of small bowel cancer survival [1], which has a poor clinical outlook as it tends to be diagnosed late.

The most popular WCE, developed and manufactured by Given Imaging [2], captures two images per second and transmits them to a recording device. The recorded images are then downloaded in a computer for review by the physician. During an exam, an average of 55,000 images are obtained, among which about 100 are from the gastrointestinal tract entrance, 4000 from the stomach, 30000 from the small intestine, and 20000 from the large intestine. A specialized doctor needs to view all the obtained images, annotate the relevant ones, and create a final report. The annotation time, which can vary between 45 and 180 minutes, is the most serious limitation of this procedure as it can miss a very localized disease [3]. Therefore, it is clear that a very important challenge of endoscopic capsule research is the automatic detection of obscure bleedings and the identification of anomalous frames. Thus, if such tool is available, the specialized doctor could focus only on the anomalous frames. The capsule manufacturers actually provide some automatic image analysis function in their software. However, performance of such tools is reported to be not satisfactory. In particular, it has been shown to yield a high false alarm rate, which limits its actual use [4].

A significant number of papers dealing with WCE image processing have recently appeared, proposing techniques to automatically discriminate digestive organs such as esophagus, stomach, small intestinal and colon ([5, 6]).

[7] describes a system for discriminating normal and abnormal tissue, whereas in [8] the authors measure the usefulness of MPEG-7 for detection of a variety of events, such as bleeding, ulcers and polyps. The problem of the automatic detection of bleeding regions has been addressed in [9], where the authors propose to use expectation-maximization clustering and Bayesian techniques. In [10], a two-steps process is proposed; the first step discriminates images with bleeding, using a block-based color saturation method; the second one refines the initial classification and increases its reliability using a pixel-based saturation-luminance analysis.

In this paper, we present an innovative technique to detect bleeding regions in WCE video. The core of the algorithm is represented by the Reed-Xiaoli (RX) detector [11], which is used to discriminate the bleeding regions from the surrounding normal tissues. In order to allow RX detector to target very specific blood areas, the data are pre-processed by means of a multi-stage filtering algorithm, and the final result is improved by means of morphological operations. Experimental results show that the proposed algorithm exhibits relatively low False Alarm Rate (FAR), substantially reducing the number of images to be analyzed to provide a diagnose proposal, and hence allowing a more widespread use of WCE.

2. ANOMALY DETECTION: THE RX ALGORITHM

The main objective of the proposed method is to discriminate between the normal internal mucosa tissue and bleeding regions, within each frame of the WCE video. This is achieved by identifying the regions that differ, in terms of spatial and/or spectral characteristics, from their surroundings. In particular, the bleeding regions are considered as isolated targets against the background; this process is known in literature as *anomaly detection*.

Anomaly detection is usually cast as a hypothesis testing problem; the typical formulation assumes that the covariance matrix of the data is unknown, and that anomalous pixels differ from the background in their mean value (see e.g.

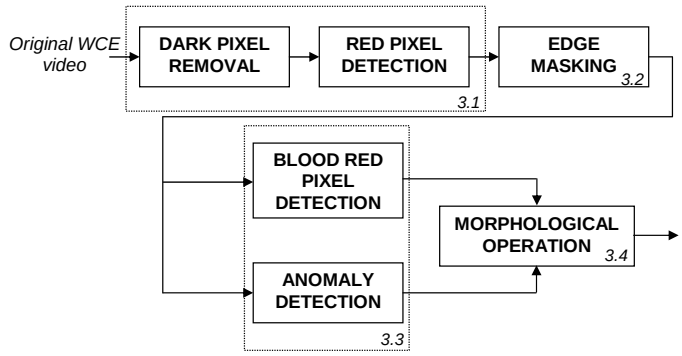

Figure 1: Block diagram of the multi-stage proposed algorithm.

[12] and [13]). Denoting as $\mathbf{x_i} = [r_i, g_i, b_i]$, $i = 1,...,N$, the RGB color representation of each pixel of WCE image, and $\mathbf{M} = [\mu_r, \mu_g, \mu_b]$ its expected value, the covariance matrix can be estimated as:

$$\widehat{C} = \frac{1}{N}\sum_{i=1}^{N}(\mathbf{x_i} - \mathbf{M})(\mathbf{x_i} - \mathbf{M})^T \quad (1)$$

where N is the total number of pixels on which the RX algorithm is evaluated. The covariance matrix $\widehat{C}$ is computed assuming that the color spectral vectors $\mathbf{x_i}$ are observations of the same random process. This is reasonable for the background pixels, but much less so for the anomalous ones. Since the anomalous pixels are typically very few, errors in these pixels hardly affect the anomaly detection performance. The generalized likelihood ratio test for declaring an anomalous pixel can be expressed in terms of the comparison with a detection threshold η_1:

$$\delta_{RX}(\mathbf{x_i}) = (\mathbf{x_i} - \mathbf{M})^T \widehat{C}^{-1}(\mathbf{x_i} - \mathbf{M}) > \eta_1 \quad (2)$$

It is interesting to notice that the RX equation in (2) performs a sort of matched filtering [14] specified by:

$$M_d(\mathbf{x_i}) = kd^T\mathbf{x_i} > \eta_2 \quad (3)$$

where d is the matched signal and k is a constant.
In general it is assumed that the background is a stationary process. However, the high non-stationarity of the WCE data, due to the presence of mucosa edges, air bubbles as well as organic residuals, makes this assumption questionable. Therefore, in the proposed method we apply a preprocessing stage that prepares the data for anomaly detection, and then run the RX algorithm.

3. THE MULTI-STAGE BLOOD DETECTION METHOD

The proposed multi-stage method is depicted in Fig. 1.

3.1 Dark pixels removal and red color pixels detection

The first stage of the proposed method (3.1 in Fig. 1) aims at discriminating image regions that could contain bleeding from those that certainly do not. This is achieved by excluding those regions that do not carry useful information for bleeding detection, i.e. the dark regions and intestinal fluids. These latter appear as yellowish to brownish semi-opaque turbid liquids often containing air bubbles as well as organic residuals. This stage is composed of two different operating blocks: *dark color pixel removal* and *red color pixels detection*. On each frame of the original WCE video, a dark pixel detector is used to remove pixels close to black color. Then, the red regions, which can represents either a normal or a bleeding tissue under various lighting conditions, are identified. In fact, the gastrointestinal images present high red hue values, except when the capsule reaches the colon, where the dominant colors become orange to yellow-green due to the presence of faecal remains.

The Hue, Saturation and Value (HSV) color space, which resembles the human vision color perception, is well suited for the processing steps described above. HSV space appears as a cone and the color set of interest for blood detection can be represented by HSV color range that spans the red hue range h, with saturation levels s that exclude the light red depending on their value v. In our simulation, we have experimentally selected $h \in [0^\circ,\ 40^\circ] \bigcup [320^\circ,\ 360^\circ]$; $s \in [0.35,\ 1.0]$; $v \in [0.25,\ 1.0]$. On the other hand, the dark pixel mask excludes the pixel with $v \in [0,\ 0.15]$.
In Fig. 2 it is possible to see the original frame (a) the dark pixel removal effect (b) and the final result of this stage (c). This latter image will be passed to the following stage for further processing.

3.2 Edge masking: the Mumford-Shah functional

Since edges represent a small portion of the whole information, and their characteristics are different from those of the background pixels, they are likely to be marked as anomalous by the RX procedure. In order to mitigate the effect of edges on the anomaly detection, we apply an edge masking process to the WCE frame processed as described in section 3.1, so as to obtain a homogenous data set that can be efficiently processed by the RX algorithm. In particular, we use an adaptive version of the Mumford-Shah (MS) functional [15].
The advantages of MS is that it allows for joint denoising and edge detection, yielding superior performance with respect to classical separated processing, and avoiding the problem of edge blurring due to filtering. Given an image, its regularized approximation and the set of discontinuities, representing edges, are obtained as the results of the MS functional minimization problem.
The edge mask is obtained applying the MS technique using as input the image elaborated in the previous stage (Fig. 2(c)). Such mask is applied on the same image, and the resulting image with removed edges is shown in Fig. 2(d). This image will be passed to the following stage for the final processing.

3.3 Blood detection

At this point, two different steps are applied independently and their outcomes are combined in order to improve the reliability of the final result.
In the first step, the *blood red color detection* stage extracts the blood red pixels exploiting the HSV color space. A bleeding region in a WCE image is characterized by the presence of a vividly red region or a dark red region. However, the red of the not bleeding region is characterized by a lower color

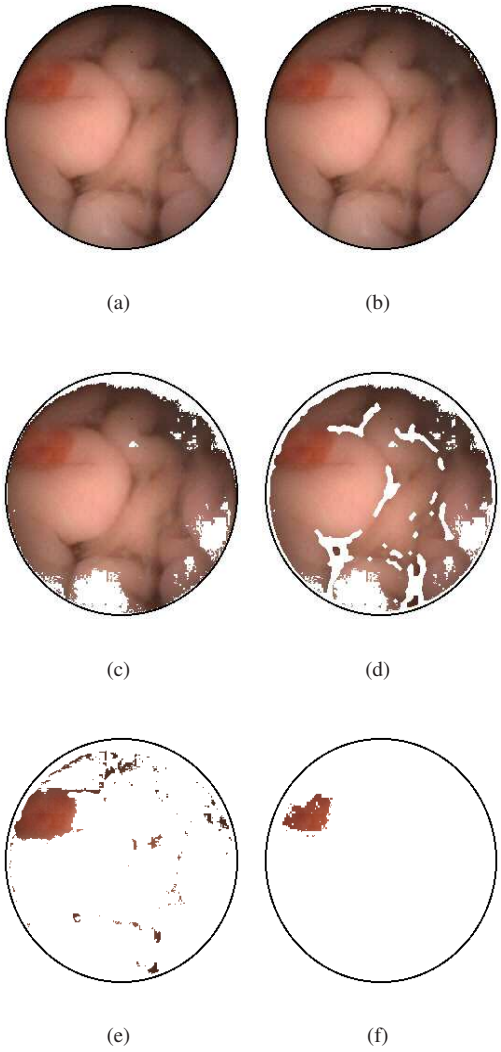

Figure 2: a) Original frame; b) Dark pixels removal result; c) Red color detection result; d) Edge masking result; e) Blood color detection result; f) RX anomaly detection result.

saturation than the bleeding area. Therefore, the detection of the bleeding region can be achieved by the detection of blood red saturated areas. In particular, pixels with HSV coordinates (h,s,v) given in (4) are marked as blood, leading to the detection of the regions shown in Fig. 2(e).
In the second step, the *RX detection algorithm* is applied, yielding to the identification of the anomalous pixels present in the preprocessed image. The result, shown in Fig. 2(f), is obtained combining the masks deriving from equations (2) and (3) respectively, where d is the spectral signature of blood in RGB color space ($[102,0,0]$ selected as in [16]).
The RX step may identify some spurious and isolated pixels as anomalous. By combining the blood red color detection with the anomaly detection results, we obtain a masking of non-bleeding areas belonging to residual anomaly areas that have not been removed by the previous stages.

3.4 Morphological operations

Finally, it is worth taking into account that bleeding areas do not appear as small and isolated areas; therefore, it is useful to remove isolated anomalous pixels [9]. To this end, the morphological erosion operation is employed. In particular, a square flat structuring element with 25 pixels area is used to discard the anomalous areas with less than 25 pixels. Fig. 3 shows the final output of the proposed blood detection technique on a given frame.

Figure 3: Final blood detection.

4. EXPERIMENTAL RESULTS

In order to evaluate the effectiveness of the proposed technique, we have carried out simulations on 11 sequences, 8 of which refer to pathological cases with different bleeding patterns and 3 referring to normal subjects. Sequences have been downloaded from *PillCam capsule endoscopy images Atlas* [17] and each sequence consists of 101 frames of size 256×256 pixels.
The results obtained with the unsupervised classification, based on the proposed method, have been compared with those yielded by manual annotation, using the False Alarm Rate (FAR) and Missed Detection Rate (MDR):

$$MDR = \frac{FN}{TP+TN+FP+FN}$$

$$FAR = \frac{FP}{TP+TN+FP+FN}$$

where TP, TN, FP, and FN represent the number of true positives, true negatives, false positives, and false negatives among all the frames respectively.
For completeness, we used also the typical measures which are widely used in the medical community to describe a diagnostic test, i.e. the *sensitivity* (SE) and *specificity* (SP) metrics [4]:

$$SE = \frac{TP}{TP+FN}$$

$$SP = \frac{TN}{TN+FP}$$

Notice that the sensitivity represents the probability of detection (PoD).
The proposed blood detection algorithm is carried out using different value of RX detection threshold η_1, and empirically setting η_2 to one half of the maximum value of $M_d(\mathbf{x_i})$ expressed in (3). We have selected η_1 so as to obtain a value of FAR on average lower than 10%, and an MDR close to 0%, as shown in Fig. 4.

$$I(x,y) = \begin{cases} \text{bloody tissue} & \{h \mid h \in [0^\circ,\ 30^\circ] \bigcup [340^\circ,\ 360^\circ]\} \bigcap \{s \mid s \in [0.5,\ 1.0]\} \bigcap \{v \mid v \in [0.25,\ 1.0]\} \\ \text{not bloody} & \text{otherwise} \end{cases} \quad (4)$$

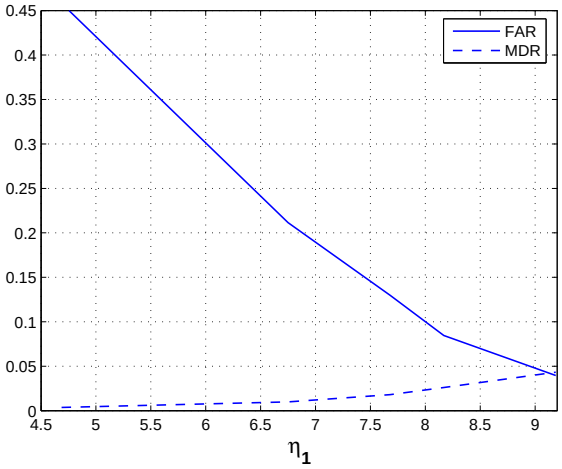

Figure 4: Average FAR and MDR versus threshold η_1, evaluated applying the proposed method to all the selected videos.

Tab. 1 shows the performance of the proposed algorithm for all the selected videos; note that for video of normal subjects, in which there are no bleeding frames, SE and SP can not be evaluated. We can notice that the algorithm exhibits a satisfactory PoD (SE) and a FAR that is on average lower than 8%; this is very useful to reduce the time spent to examine the video sequence. Our experimental results show that the proposed method achieves on average 92% and 88% of sensitivity and specificity respectively.
It is important noticing that direct comparison with previously proposed methods is not possible due to the different data sets employed; however, the results of the proposed algorithm are comparable to those reported in [18].

Table 1: SE, SP, FAR and MDR of the proposed algorithm applied to 8 videos with different bleeding patterns (bleeding video) and 3 videos of normal subjects (normal video) (341 bleeding frames + 770 normal frames).

	SE	SP	FAR	MDR
bleeding video1	0.76	0.73	0.13	0.14
bleeding video2	1	0.92	0.08	0
bleeding video3	0.67	0.89	0.099	0.02
bleeding video4	0.93	0.93	0.03	0 .04
bleeding video5	0.94	0.82	0.02	0.05
bleeding video6	0.82	0.97	0.03	0.02
bleeding video7	1	0.57	0.09	0
bleeding video8	0.95	0.70	0.18	0.02
normal video1	-	-	0.11	0
normal video2	-	-	0.11	0
normal video3	-	-	0.06	0
average	0.92	0.88	0.08	0.03

5. CONCLUSIONS

This paper proposes an algorithm for automatic analysis of bleeding patterns in WCE images. In particular, it implements a blood detection algorithm based on color modeling, edge masking and RX detection. The core of the proposed algorithm is the RX detector, which is implemented on pre-processed images. The simulation results reveal that the algorithm is effective at achieving a satisfactory PoD along with a relatively low FAR. Therefore, it is expected to substantially reduce the number of images to be manually analyzed to provide a diagnose proposal, allowing a more widespread use of WCE. It is worth noticing that the used sequences are compressed, and as a consequence the obtained results can be impaired by the distortion introduced by compression. Future developments will include the algorithm validation on uncompressed data, and the exploitation of the correlation between adjacent frames in order to improve the performance of the RX detection stage.

6. ACKNOWLEDGMENT

The authors would like to thank Dr. M. Pennazio (Unit of Gastroenterology, Ospedale San Giovanni AS, Turin, Italy), for his valuable medical support.
This work was supported by the *Programma di Ricerca Sanitaria Finalizzata 2008-2009*, Regione Piemonte.

REFERENCES

[1] M. Coimbra, M. Mackiewicz, M. Fisher, C. Jamieson, J. Soares, and J.P. Silva Cunha, "Computer vision tools for capsule endoscopy exam analysis," in *Eurasip NewsLetter*, Mar. 2007, vol. 18/1, pp. 1–19.

[2] Web page of Given Imaging, *http://www.givenimaging.com*.

[3] E. Rondonotti, J. M. Herrerias, M. Pennazio, A. Caunedo, M. Mascarenhas-Saraiva, and R. de Franchis, "Complications, limitations, and failures of capsule endoscopy: a review of 733 cases," *Gastrointestinal Endoscopy, Elsevier*, vol. 62, pp. 712 – 716, Nov 2005.

[4] C. Signorelli, F. Villa, E. Rondonotti, C. Abbiati, G. Beccari, and R. de Franchis, "Sensitivity and specificity of the suspected blood identification system in video capsule enteroscopy," in *Endoscopy*, 2005, vol. 37/12, pp. 1170 – 1173.

[5] M. Coimbra, P. Campos, and J.P. Silva Cunha, "Topographic segmentation and transit time estimation for endoscopic capsule exams," in *Proc. of IEEE ICASSP 2006, Toulouse, France*, May 2006, vol. 2, pp. 1164 – 1167.

[6] Lee Jeongkyu, Oh JungHwan, , Yuan Xiaohui, and Tang Shou-Jiang, "Automatic classification of digestive organs in wireless capsule endoscopy videos," in *SAC '07: Proceedings of the 2007 ACM symposium on Applied computing*, 2007, pp. 1041–1045.

[7] N. Bourbakis, "Detecting abnormal patterns in wce images," in *5th IEEE Symposium on Bioinformatics and Bioengineering (BIBE05)*, 2005, pp. 232–238.

[8] M.T. Coimbra and J.P.S Cunha, "Mpeg-7 visual descriptorscontributions for automated feature extraction in capsule endoscopy," *IEEE Transactions on Circuits and Systems for Video Technology*, vol. 16, pp. 628 – 637, 2006.

[9] S. Hwang, J. Oh, J. Cox, S. J. Tang, and H. F. Tibbals, "Blood detection in wireless capsule endoscopy using expectation maximization clustering," in *Medical Imaging 2006. Proc. of the SPIE, Volume 6144, pp. 577-587.*, Mar. 2006, vol. 6144, pp. 577–587.

[10] Phooi Yee Lau and Paulo Lobato Correia, "Detection of bleeding patterns in wce video using multiple features," in *Annual International Conference of the IEEE Engineering in Medicine and Biology Society*, Aug 2007, pp. 5601 – 5604.

[11] I.S. Reed and X. Yu, "Adaptive multiband cfar detection of an optical pattern with unknown spectral distribution," in *IEEE Trans. on Acoustics, Speech and Signal Processing*, Oct. 1990, vol. 38/10, pp. 1760 – 1770.

[12] D.W.J. Stein, S.G. Beaven, L.E. Hoff, E.M. Winter, A.P. Schaum, and A.D. Stocker, "Anomaly detection from hyperspectral imagery," *IEEE Signal Processing Magazine*, vol. 19, no. 1, pp. 58–69, Jan 2002.

[13] B. Penna, T. Tillo, E. Magli, and G. Olmo, "Progressive 3-d coding of hyperspectral images based on JPEG 2000," in *IEEE Geoscience and Remote Sensing Letters*, Jan. 2006, vol. 3/1, pp. 125 – 129.

[14] Chein-I Chang and Shao-Shan Chiang, "Anomaly detection," *IEEE Transactions Geoscience and Remote Sensing*, vol. 40, pp. 1314–1325, June 2002.

[15] D. Mumford and J. Shah, "Optimal approximations by piecewise smooth functions and associated variational problems," in *Comm. Pure Appl. Math*, 1989, vol. 42, pp. 577 – 685.

[16] Web Page of Stanford univesity, *http://www.stanford.edu/ callisto/colors.html*.

[17] Web Page of capsule endoscopy, *http://capsuleendoscopy.org*.

[18] Yun Sub Jung, Young Ho Kim, and Dong Ha Leeand Jong Hyo Kim, "Active blood detection in a high resolution capsule endoscopy using color spectrum transformation," in *International Conference on BioMedical Engineering and Informatics, 2008. BMEI 2008.*, May 2008, vol. 1, pp. 859–862.